PHYSICAL REVIEW D **88,** 074032 (2013)

Hybrid scheme for heavy flavors: Merging the fixed flavor number scheme and variable flavor number scheme

A. Kusina,[1,*] F. I. Olness,[1,†] I. Schienbein,[2,‡] T. Ježo,[3,§] K. Kovařík,[4,‖] T. Stavreva,[2,¶] and J. Y. Yu[1,**]

[1]*Southern Methodist University, Dallas, Texas 75275, USA*

[2]*Laboratoire de Physique Subatomique et de Cosmologie, Université Joseph Fourier/CNRS-IN2P3/INPG, 53 Avenue des Martyrs, 38026 Grenoble, France*

[3]*Department of Physics, University of Durham, Durham DH1 3LE, United Kingdom and Department of Mathematical Sciences, University of Liverpool, Liverpool L69 3BX, United Kingdom*

[4]*Institute for Theoretical Physics, Karlsruhe Institute of Technology, Karlsruhe D-76128, Germany*

(Received 1 July 2013; published 28 October 2013)

We introduce a hybrid variable flavor number scheme for heavy flavors, denoted H-VFNS, which incorporates the advantages of both the traditional variable flavor number scheme as well as the fixed flavor number scheme (FFNS). By including an explicit N_F dependence in both the parton distribution functions (PDFs) and the strong coupling constant α_S, we generate coexisting sets of PDFs and α_S for $N_F = \{3, 4, 5, 6\}$ at any scale μ that are related analytically by the $\overline{\text{MS}}$ matching conditions. The H-VFNS resums the heavy quark contributions and provides the freedom to choose the optimal N_F for each particular data set. Thus, we can fit selected HERA data in a FFNS framework, while retaining the benefits of the VFNS to analyze LHC data at high scales. We illustrate how such a fit can be implemented for the case of both HERA and LHC data.

DOI: 10.1103/PhysRevD.88.074032 PACS numbers: 12.38.−t, 13.60.Hb, 14.65.Dw

I. INTRODUCTION

Parton distribution functions (PDFs) provide the essential link between the theoretically calculated partonic cross sections and the experimentally measured physical cross sections involving hadrons and mesons. A good understanding of this link is crucial if we are to make incisive tests of the standard model, and search for subtle deviations which might signal new physics.

For precision analyses of PDFs, the heavy quarks (charm, bottom, and top) must be properly taken into account; this is a nontrivial task due to the different mass scales which enter the theory. There is extensive literature devoted to this question, and various heavy flavor schemes have been devised which are used in modern global analyses of parton distribution functions. The CTEQ global analyses of PDFs in nucleons [1,2] and nuclei [3,4] employ as a default[1] the Aivazis-Collins-Olness-Tung (ACOT) scheme [5,6] and refinements of it [7,8]. Extensions of the ACOT scheme beyond next-to-leading order (NLO) [6,9] were recently presented in Refs. [10,11]. The general ACOT scheme has also been applied to the case of deep inelastic scattering (DIS) jet production [12,13] and pp induced heavy quark production [14]. The default scheme of the Martin-Stirling-Thorne-Watt (MSTW) PDFs [15] is the Thorne-Roberts (TR) factorization scheme [16,17] and the NNPDF Collaboration uses the fixed-order next-to-leading logs (FONLL) method [18] applied to DIS [19] in its most recent PDF studies [20,21]. The ACOT, TR, and FONLL schemes are examples of (general mass) variable flavor number schemes (VFNS). Other groups like ABKM/ABM [22,23] and GJR/JR [24,25] utilize the fixed flavor number scheme (FFNS) as their default option, but include an option for other N_F values [22]. For recent reviews of the schemes see, e.g., [26,27] and Sec. 22 in [28].

The ACOT scheme is based on the proof of factorization with massive quarks by Collins [29] which incorporates the flexibility of introducing separate matching and switching scales (see Secs. II and III). This possibility has been discussed in the literature for some time [19,26,27,30]. However, it is technically more complicated and has never been implemented in a global analysis framework employing the ACOT scheme. In this paper we study the VFNS in its most general formulation, with separate matching and switching scales, and denote it as the hybrid variable flavor number scheme (H-VFNS) in order to clearly distinguish it from the *traditional* VFNS.

In the H-VFNS we generate *coexisting* sets of PDFs $f_a(x, \mu, N_F)$ and the strong coupling constant $\alpha_s(\mu, N_F)$ with $N_F = \{3, 4, 5, 6\}$ which are related analytically by the precise $\overline{\text{MS}}$ matching conditions. This provides maximal flexibility, both in a global analysis and for application of these PDFs, to choose the optimal subscheme (i.e. the value of N_F) in which to compute a

*akusina@smu.edu
†olness@smu.edu
‡schien@lpsc.in2p3.fr
§T.Jezo@liverpool.ac.uk
‖kovarik@particle.uni-karlsruhe.de
¶stavreva@lpsc.in2p3.fr
**yu@physics.smu.edu

[1]In addition to the default scheme, many groups also provide sets of PDFs obtained in other heavy flavor schemes.

given observable. The freedom of the H-VFNS allows an improved description of heavy flavor data sets in a wide kinematic range.

The rest of this paper is organized as follows. In Sec. II we present a brief review of existing heavy flavor schemes before we introduce our new H-VFNS in Sec. III. In Sec. IV we investigate the N_F dependence of the PDFs and α_s, followed by a discussion of the N_F dependence of physical structure functions in Sec. V. In Sec. VI we present an example of how the H-VFNS scheme could be employed for a simultaneous study of low-scale data from HERA and high-scale data from the LHC as they might enter a global analysis of PDFs. Finally, in Sec. VII we present our conclusions. Technical details concerning the evolution of α_s and the PDFs as well as the matching conditions between sets with different N_F have been relegated to the appendix.

II. BRIEF REVIEW OF HEAVY FLAVOR SCHEMES

There are several basic requirements that any complete theoretical description of heavy quarks must satisfy in the context of perturbative QCD (pQCD) to be valid in the full kinematic range from low to high energies [26,29]. In particular, we focus on the following three:

(1) For energy scales $\mu \ll m$, the heavy quark of mass m should decouple from the theory.
(2) For energy scales $\mu \gg m$, physical observables must be infrared safe (IR safe).
(3) Heavy quark mass effects should be properly taken into account.

We now discuss/review some of the heavy flavor schemes used in the literature in the light of the three basic requirements.

In the following, we denote a factorization (renormalization) scheme with N_F (N_R) active quark flavors in the initial state (in quark loops) by $\mathrm{S}^{(N_F,N_R)}$. If not stated otherwise, we set $N_F = N_R$ and write $\mathrm{S}^{(N_F)}$.

A. Fixed flavor number scheme

A single scheme $\mathrm{S}^{(N_F)}$ with a fixed number of active quark partons N_F is called a fixed flavor number scheme. For example, in the $N_F = 3$ FFNS, $\mathrm{S}^{(3)}$, the gluon and the three light quarks (u, d, s) are treated as active partons whereas the heavy quarks are *not* partons. They can only be produced in loops and in the final state and their masses are fully retained in the perturbative fixed order calculations. Similarly, it is possible to define a $N_F = 4$ FFNS, $\mathrm{S}^{(4)}$, and a $N_F = 5$ FFNS, $\mathrm{S}^{(5)}$.

The FFNS satisfies the requirements 1 and 3. In particular, the final state kinematics are exactly taken into account. Conversely, the FFNS is not IR safe because logarithms of the heavy quark mass $\alpha_s \ln(\mu/m)$ arise in each order of perturbation theory which will become large for asymptotic energies $\mu \gg m$ so that they eventually spoil the convergence of the perturbation series in α_s. Therefore, the FFNS cannot be reliably extended up to high energy scales such as those required for analysis of the LHC data.

Despite the lack of IR safety, the FFNS is widely used because it is conceptually simple and a proper treatment of the final state kinematics is crucial close to the heavy quark production threshold and for exclusive studies of heavy quark production.

B. Variable flavor number scheme

A variable flavor number scheme is composed of a set of fixed flavor number schemes $\mathrm{S}^{(N_F)}$ with different N_F values. The *matching scale* $\mu = \mu_M^{(N_F)}$ specifies the scale at which the PDFs and α_s in the scheme with $N_F + 1$ flavors are related to those with N_F flavors. The matching scales are of the order of the heavy quark mass $\mu_M^{(N_F)} \simeq m_{N_F}$ ($N_F = 4, 5, 6$) in order to avoid large logarithms in the perturbatively calculable matching conditions. The PDFs, α_s, and observables are computed in a subscheme $\mathrm{S}^{(N_F)}$, where $N_F = 3, 4, 5, 6$ is determined by the energy scale μ. We write this schematically as

$$\mathrm{S}^{(3)} \overset{\mu_M^{(4)}}{\longrightarrow} \mathrm{S}^{(4)} \overset{\mu_M^{(5)}}{\longrightarrow} \mathrm{S}^{(5)} \overset{\mu_M^{(6)}}{\longrightarrow} \mathrm{S}^{(6)}. \tag{1}$$

By construction, a VFNS satisfies heavy quark decoupling (requirement 1) since this is respected by the individual schemes $\mathrm{S}^{(N_F)}$ from which the VFNS is comprised. Furthermore, a VFNS is IR safe (requirement 2) because it resums the $\alpha_s \ln(\mu/m_{N_F})$ terms to all orders via the contribution from the heavy quark PDFs; hence, it can be reliably extended to the region $\mu/m_{c,b} \to \infty$.

The most delicate point to satisfy is the proper treatment of the heavy quark mass (requirement 3) [29]:

(i) In the VFNS, since the UV counterterms are the same as in the $\overline{\mathrm{MS}}$ scheme, the evolution equations for the PDFs and α_s are *exactly* those of a pure massless $\overline{\mathrm{MS}}$ scheme with N_F active flavors; therefore, the information on the heavy quark masses enters the PDF evolution only via the matching conditions between two subschemes.[2]
(ii) The VFNS formalism allows all quark masses to be retained in the calculation of the Wilson coefficients. While it is common to neglect the masses of the lighter quarks for practical purposes, this simplification is not necessary for the application of the VFNS; hence, the VFNS fully retains all $\mathcal{O}(m^2/\mu^2)$ contributions. Furthermore, multiple heavy quark masses can be treated precisely without loss of accuracy, and this result is independent of whether the heavy quark masses are large or small;

[2]For details about the $\overline{\mathrm{MS}}$ evolution of the heavy quarks see Refs. [31,32].

hence, we have no difficulty addressing contributions of m_c and m_b simultaneously in the VFNS.

(iii) Of course, the heavy quark masses can also be retained in the calculation of the final state phase space of a given partonic subprocess. Here, the difficulty arises that "collinear" heavy quarks in the evolution equations do not appear in the partonic subprocesses and their effect on the phase space is therefore not taken into account. For example, in DIS, the second heavy quark produced by a gluon splitting is "lost" in the leading order $\gamma^\star + c \to c$ subprocess and theoretical calculations in a VFNS can overshoot the data close to the $c\bar{c}$ production threshold, i.e., at low Q^2 and large x. The problem can be overcome by incorporating the kinematical effect of the second heavy quark via a slow rescaling variable resulting in the ACOT$_\chi$ scheme.[3] Subsequently, this procedure has also been adopted by the MSTW group [17].

(iv) The ACOT$_\chi$ prescription provides a practical solution for the purpose of improving the quality of global analyses of PDFs in the VFNS since DIS structure function data—forming the backbone of such analyses—are better described at low Q^2.

However, there are some shortcomings of the χ prescription: (i) The convolution variable (at LO, the slow-rescaling variable) is not unique and different versions have been investigated in the literature [33]. (ii) As a matter of principle, production thresholds for more than one heavy quark pair (say 2 or 3 heavy quark pairs) cannot be captured with a single slow-rescaling variable. Numerically, however, this will have negligible consequences (at NNLO precision). (iii) Most importantly, a corresponding prescription has not yet been formulated for the hadroproduction of heavy quarks [34–37] or other less inclusive observables. Note, these shortcomings of the χ prescription do not apply to the general ACOT prescription.

The problems satisfying requirement 3 can be overcome/reduced by switching to the $S^{(4)}$ scheme not at the charm mass but at a larger scale. This possibility will be discussed in the next section.

III. HYBRID VARIABLE FLAVOR NUMBER SCHEME

The traditional VFNS introduced in the previous section can be generalized by introducing, in addition to the matching scales $\mu_M^{(N_F)}$, separate *switching scales* $\mu_S^{(N_F)}$. The switching scale $\mu_S^{(N_F)}$ prescribes where the transition from the scheme with N_F flavors to the one with $N_F + 1$ flavors is performed. Below the switching scale $[\mu < \mu_S^{(N_F)}]$ *physical observables* are calculated in the $\mathrm{S}^{(N_F)}$ scheme, and above the switching scale $[\mu_S^{(N_F)} < \mu]$ they are calculated in the $\mathrm{S}^{(N_F+1)}$ scheme. Thus, the H-VFNS is a series of subschemes specified by

$$\mathrm{S} = \begin{cases} \mathrm{S}^{(3)}; & \mu \le \mu_S^{(4)} \\ \mathrm{S}^{(4)}; & \mu_S^{(4)} < \mu \le \mu_S^{(5)} \\ \mathrm{S}^{(5)}; & \mu_S^{(5)} < \mu \le \mu_S^{(6)} \\ \mathrm{S}^{(6)}; & \mu_S^{(6)} < \mu \end{cases}. \tag{2}$$

We refer to this scheme as the hybrid variable flavor number scheme (H-VFNS) in order to clearly distinguish it from the traditional VFNS in which the matching and the switching (transition) scales are equal. Indeed, in all practical applications to date these scales have been identified with the heavy quark masses: $\mu_M^{(N_F)} = \mu_S^{(N_F)} = m_{N_F}$; while this choice leads to considerable simplifications at the technical level, it also brings some disadvantages which we will discuss below.[4] The theoretical basis for the implementation of the presented H-VFNS follows the general formulation of the ACOT scheme given (and proven) in Ref. [29].

The essential technical step to implement the H-VFNS is to add an explicit dependence on the number of active flavors, N_F, in both the PDFs $f_a(x, \mu, N_F)$ and the strong coupling $\alpha_S(\mu, N_F)$. This concept is illustrated notationally as

$$f_i(x, \mu) \to f_i(x, \mu, N_F), \qquad \alpha_s(\mu) \to \alpha_s(\mu, N_F),$$

and we illustrate this schematically in Fig. 1 where we explicitly see the coexistence of PDFs and α_S for different N_F values.[5]

Instead of a single PDF, we will have a set of four coexisting PDFs, $f_a(x, \mu, N_F)$ with $N_F = \{3, 4, 5, 6\}$, that are related analytically by the $\overline{\mathrm{MS}}$ matching conditions (see Appendix A 2). Therefore, by knowing the PDFs for a specific N_F branch, we are able to compute the related PDFs for any other number of active flavors.[6] Likewise, we have a set of four coexisting strong couplings, $\alpha_S(\mu, N_F)$

[3]The details of the ACOT$_\chi$ factorization scheme are in Ref. [8], and the factorization proof for S-ACOT$_\chi$ was demonstrated in Ref. [10].

[4]The choice $\mu_M^{(N_F)} = m_{N_F}$ eliminates terms of the form $\ln(\mu/m_{N_F})$ in the matching conditions. Note, that we generally prefer to choose $\mu_M^{(N_F)} \le \mu_S^{(N_F)}$; technically, we have the freedom to choose $\mu_M^{(N_F)} > \mu_S^{(N_F)}$, but this would require a numerically unstable DGLAP "backward evolution" from the matching scale $\mu_M^{(N_F)}$ down to the switching scale $\mu_S^{(N_F)}$.

[5]The use of the 6-flavor α_S in the ratio in Fig. 1 at low scales is just for illustration; for realistic calculations in the H-VFNS the 6-flavor α_S is used only above the $\mu_S^{(6)}$ switching scale. Also the number of flavors used in α_S and PDFs is always matched.

[6]This analytic relation is in contrast to, for example, the CTEQ5M $N_F = \{3, 4, 5\}$ flavor fits [38], where each N_F fit represents a separate phenomenological fit to the data set. Separately, the MSTW $N_F = \{3, 4, 5\}$ flavor fits of Refs. [39,40] are related by $\overline{\mathrm{MS}}$ matching conditions.

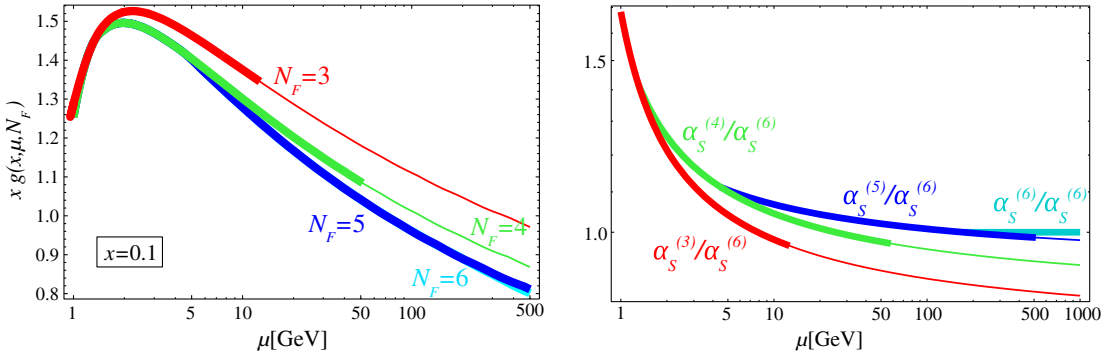

FIG. 1 (color online). Schematic of a H-VFNS: PDF (left) and α_S (right) vs μ for a selection of N_F values. The preferred range of each N_F branch is indicated by the thicker line. Thus, $f_i(x, \mu, N_F = 3)$ can be used slightly above the m_c transition, but for very large μ scales the $N_F = 4, 5, 6$ branches are preferred as these resum the m_c mass singularities.

for $N_F = \{3, 4, 5, 6\}$, that are also related analytically by the $\overline{\text{MS}}$ matching conditions (see Appendix A 1).

A. Generating the PDFs and α_s in the H-VFNS

These PDFs and α_s are computed using the following prescription.

(1) Parametrize the PDFs at a low initial scale $\mu_0 = Q_0 \sim 1$ GeV; as this is below the $m_{c,b,t}$ thresholds, this would correspond to $N_F = 3$. We also choose an initial value for $\alpha_s(\mu_0, N_F = 3)$ at the same scale.[7]

(2) Starting at an initial scale μ_0 with $N_F = 3$, we evolve the PDFs using the Dokshitzer-Gribov-Lipatov-Altarelli-Parisi (DGLAP) evolution equations and $\alpha_s(\mu, N_F)$ with the renormalization group equations up to $\mu_{\max}$. We thus obtain $f_a(x, \mu, N_F = 3)$ and $\alpha_s(\mu, N_F = 3)$ for scales $\mu \in [\mu_0, \mu_{\max}]$.

(3) At $\mu = m_c$ we use the $\overline{\text{MS}}$ matching conditions to compute both the $N_F = 4$ PDFs and α_s using the $N_F = 3$ results. We then use the $N_F = 4$ evolution equations to obtain $f_a(x, \mu, N_F = 4)$ and $\alpha_s(\mu, N_F = 4)$ up to $\mu_{\max}$.

(4) At $\mu = m_b$ we again use the $\overline{\text{MS}}$ matching conditions to compute both the $N_F = 5$ PDFs and α_s using the $N_F = 4$ results. We then use the $N_F = 5$ evolution equations to obtain $f_a(x, \mu, N_F = 5)$ and $\alpha_s(\mu, N_F = 5)$ up to $\mu_{\max}$.

(5) At $\mu = m_t$ this procedure can be repeated again with $N_F = 6$ for the top quark.[8]

Because all the $N_F = \{3, 4, 5, 6\}$ results for the PDFs $f_a(x, \mu, N_F)$ and the strong coupling $\alpha_S(\mu, N_F)$ are retained, the user has the freedom to choose which N_F to use for a particular calculation.[9] However, note that the number of active flavors used in α_S and in PDFs is always the same.

B. Properties of the H-VFNS

Having generated a set of N_F-dependent PDFs and strong couplings, we highlight two important properties.

(1) The PDFs and strong couplings with different N_F flavors coexist simultaneously.

(2) The PDFs and strong couplings with one N_F value have a precise analytic relation to those with a different N_F value which is specified by the appropriate evolution equations and the $\overline{\text{MS}}$ boundary conditions at $\mu = m_{c,b,t}$ (cf., the Appendix).

Property (1) allows us to avoid dealing with an N_F flavor transition should it happen to lie right in the middle of a data set. For example, if we analyze the HERA F_2^{charm} data[10] which covers a typical range of $Q \sim [3, 8]$ GeV, if we were to use the traditional VFNS then the N_F transition between 4 and 5 flavors would lie right in the middle of the analysis region; clearly this is very inconvenient for the analysis. Because we can specify the number of active flavors N_F in the H-VFNS, we have the option to *not* activate the b-quark in the analysis even when $\mu > m_b$; instead, we perform all our calculations of F_2^{charm} using $N_F = 4$ flavors. This will avoid any potential discontinuities in the PDFs and α_s in contrast to the traditional VFNS which forces a transition to $N_F = 5$ at the b-quark mass.

Property (2) allows us to use the $N_F = 4$ PDF $f_i(x, \mu, N_F = 4)$ extracted from the F_2^{charm} data set and relate this to $N_F = 5$ and $N_F = 6$ PDFs that can be applied at high μ scales for LHC processes. In this example note

[7]In practice, we obtain $\alpha_s(\mu_0, N_F = 3)$ by evolving the world average [41] $\alpha_s(M_Z, N_F = 5) = 0.1184$ down to μ_0 using the renormalization group equation as described in Appendix A 1.

[8]For maximum generality, we include the $N_F = 6$ case of the top quark; in practice, even for LHC processes there is little need to resum these contributions.

[9]Note that there is a residual dependence on the involved matching and switching scales (which is also present in traditional VFNS). This is further discussed in Appendix A 2.

[10]Consider, for example, the data set of Ref. [42].

that all the HERA F_2^{charm} data (both above and below m_b) influence the $N_F = 5$ and $N_F = 6$ PDFs used for the LHC processes.[11]

C. Challenges resolved

We can now see how this H-VFNS overcomes the challenges noted above. While the traditional VFNS forced the user to transition from $N_F = 4$ to $N_F = 5$ at $\mu = m_b$ (for example), because the H-VFNS approach retains the N_F information we have the freedom to use the $N_F = 4$ calculation for μ scales even above m_b.

The H-VFNS also shares the benefits of the FFNS in that we can avoid a N_F transition which might lie in the middle of a data set. Furthermore, while the FFNS cannot be extended to large scales due to the uncanceled logs, the H-VFNS can be used at high scales (such as for LHC processes) because we retain the freedom to switch N_F values and resum the additional logs where they are important.

Additionally, the H-VFNS implementation gives the user maximum flexibility in choosing where to switch between the N_F and $N_F + 1$ calculations. Not only can one choose different switching points for different processes (as sketched above), but also we can make the switching point dependent on the kinematic variables of the process. For example, the production thresholds for charm/bottom quarks in DIS are given in terms of the photon-proton center-of-mass energy $W^2 \simeq Q^2(1-x)/x$; thus, we could use this to define our switching scales.

An important operational question is, how far above the $\mu = m_Q$ can we reliably extend a particular N_F framework? We know this will have mass singular logs of the form $\alpha_s \ln(\mu/m_Q)$, so these will eventually spoil the perturbative expansion of the coefficient functions. We just need to ensure that we transition to the $N_F + 1$ result before these logs obviate the perturbation theory. We will investigate this question numerically in Sec. V.

D. Relation to previous work

In closing we want to note that many of the ideas that we build upon here with the H-VFNS have been present in the literature for some time. The proof of factorization paper by Collins [29] incorporates the flexibility of introducing separate matching and switching scales; applications to the ACOT scheme were outlined in Ref. [30]; and Ref. [26] provides a recent review of the situation. The separate N_F sets of the MSTW Collaboration [39] are precisely defined by the $\overline{\text{MS}}$ matching conditions [44] at $\mathcal{O}(\alpha_s)$. This is extended to higher order for MSTW [40] and ABKM/ABM [22]. Additionally, the NNPDF group provides PDF sets with different numbers of active flavors in Refs. [20,21] for NLO and NNLO. The phenomenological implications of coexisting N_F PDF sets has been investigated in the MSTW and NNPDF frameworks [45,46]. The extension of the ACOT scheme beyond NLO, where the PDF and α_S discontinuities appear, was presented in Ref. [11]. Putting these pieces together, and including the explicit N_F dependence, allows us to construct a tractable implementation of the H-VFNS with user-defined switching scales.

Operationally, we are able to provide maximum flexibility with only a minimal extension of the PDF. A fully general framework as described in Ref. [30] would require a separate PDF grid (and associated evolution) for each data set with a distinct matching or switching scale. With the implementation outlined in the H-VFNS we are able to implement this economically with only three PDF grids for $N_F = \{3, 4, 5\}$; this is possible for a number of reasons as outlined below.

While we have imposed the choice $\mu_M^{(N_F)} = m_{N_F}$, we demonstrate in Appendix A 2 that when the matching conditions are implemented correctly, particularly at higher orders, the physical influence of this matching condition is minimal. On physical grounds, the natural choice for the switching scale is at or above the heavy quark mass scale $\mu_S^{(N_F)} \geq m_{N_F}$. Additionally, it is generally preferred to have the switching scale above the matching scale $\mu_M^{(N_F)} \leq \mu_S^{(N_F)}$ as this avoids the need for backward evolution. Our implementation of the H-VFNS with $m_{N_F} = \mu_M^{(N_F)} \leq \mu_S^{(N_F)}$ naturally accommodates these choices.

Therefore, our H-VFNS implementation economically requires only three PDF grids (for $N_F = \{3, 4, 5\}$), yet provides the user flexibility to use any switching scale, and the choice of the fixed matching scale $\mu_M^{(N_F)} = m_{N_F}$ has minimal impact on the physical results.

IV. N_F DEPENDENCE OF THE PDFS AND α_s

In this study we are using an initial PDF parametrization based on the nCTEQ "decut3" set of Ref. [47]. We use quark masses of $m_c = 1.3$ GeV, $m_b = 4.5$ GeV, and $m_t = 175$ GeV, with a starting scale of $Q_0 = 1.2$ GeV which allows us to examine the charm threshold. The full set of $N_F = \{3, 4, 5, 6\}$ PDFs is generated as described above using the $\overline{\text{MS}}$ matching conditions applied at the quark

[11] Conceptually, the HERA data above the bottom mass ($m_b < \mu$) on the $N_F = 4$ branch is "backward evolved" to the matching point $\mu_M^{(5)} = m_b$, and then "forward evolved" for $N_F = 5$ and $N_F = 6$. We outline this procedure in more detail in Sec. VI. In particular, we show how such a fit can be performed using only forward evolution, thus avoiding a (potentially unstable) numerical backward evolution [43].

mass values.[12] The details of the matching are described in Appendix A.

A. N_F dependence of the PDFs

We begin by illustrating the effect of the number of active flavors N_F on the PDFs, $f_i(x, \mu, N_F)$. One of the simplest quantities to examine is the momentum fraction $[\int_0^1 x f_i(x) dx]$ carried by the PDF flavors as a function of the μ scale.

Figure 2 shows the gluon and heavy quark momentum fractions as a function of the μ scale. For very low μ scales all the curves coincide by construction; when $\mu < m_{c,b,t}$ the charm, bottom, and top degrees of freedom will "deactivate" and the $N_F = 4, 5, 6$ results will reduce to the $N_F = 3$ result.

As we increase the μ scale, we open up new channels. For example, when $\mu > m_c$ the charm channel activates and the DGLAP evolution will generate a charm PDF via the $g \to c\bar{c}$ process. Because the overall momentum sum rule must be satisfied $[\sum_i \int_0^1 x f_i(x) dx = 1]$, as we increase the momentum carried by the charm quarks, we must decrease the momentum carried by the other partons. This interplay is evident in Fig. 2. In Fig. 2(a), we see that for $\mu = 1000$ GeV, the momentum fraction of the $N_F = 4$ gluon is decreased by $\sim 4\%$ as compared to the $N_F = 3$ gluon. Correspondingly, in Fig. 2(b) we see that at $\mu = 1000$ GeV, the momentum fraction of the charm PDF is $\sim 4\%$. Thus, when we activate the charm in the DGLAP evolution, this depletes the gluon and populates the charm PDF via $g \to c\bar{c}$ process.

In a similar manner, comparing the momentum fraction of the $N_F = 5$ gluon to the $N_F = 4$ gluon at $\mu = 1000$ GeV we see the former is decreased by $\sim 3\%$; in Fig. 2(b) we see that at $\mu = 1000$ GeV the momentum fraction of the bottom PDF is $\sim 3\%$.

The gluon PDF is primarily affected by the heavy N_F channels as it couples via the $g \to c\bar{c}, b\bar{b}, t\bar{t}$ processes. The effect on the light quarks $\{u, d, s\}$ is minimal as these only couple to the heavy quarks via higher order processes $(u\bar{u} \to g \to c\bar{c})$. This property is illustrated in Fig. 3 where we display the u and $\bar{u}$ quark momentum for different N_F values. While the N_F variation yields a $\sim 8\%$ momentum fraction shift for the gluon, the total shift of the u quark is only $\sim 1\%$ of the momentum fraction.[13]

B. N_F dependence of α_s

The PDFs are only one piece of the full calculation; another essential ingredient is the strong coupling constant $\alpha_S(\mu, N_F)$. The running coupling is sensitive to

[12]These N_F-dependent PDFs are available on the nCTEQ web page at http://www.HEPForge.org.

[13]For example, in Fig. 3(a), we see the momentum fraction change from $\sim 20\%$ for $N_F = 3$ to $\sim 19\%$ for $N_F = 6$.

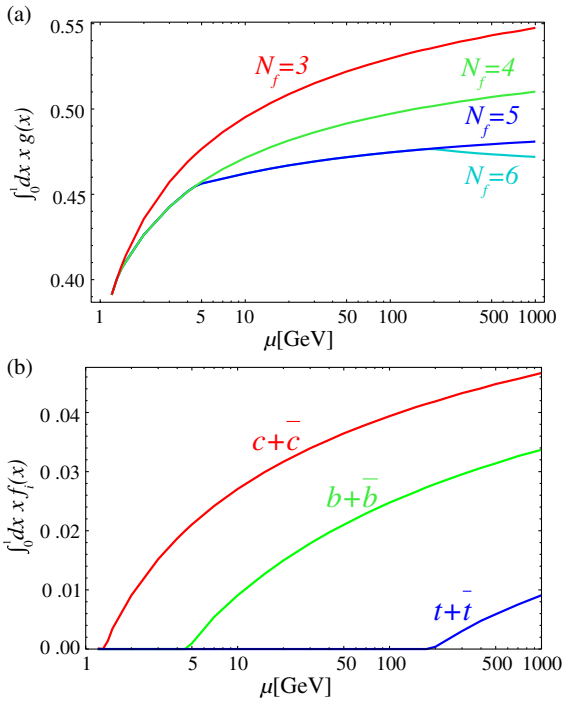

FIG. 2 (color online). (a) Gluon momentum fraction; (b) momentum fraction for $c + \bar{c}$, $b + \bar{b}$ and $t + \bar{t}$ quarks. The results have been obtained using NLO PDFs ($\overline{\text{MS}}$) with a 2-loop α_S.

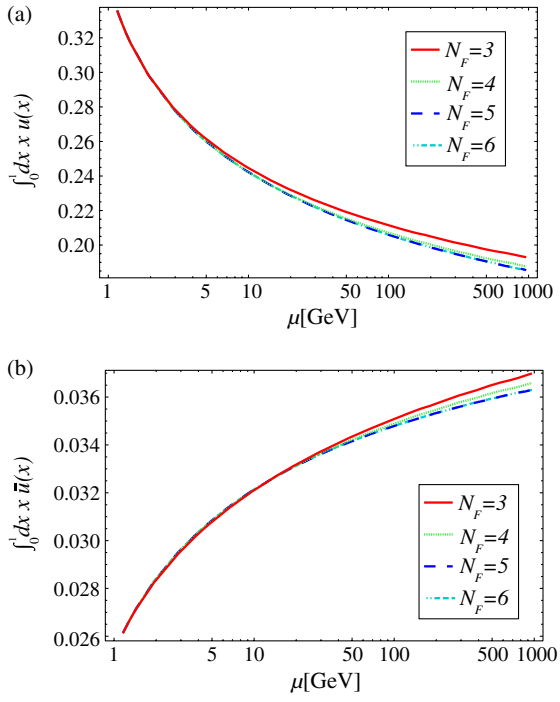

FIG. 3 (color online). Momentum fraction carried by the (a) u quark and (b) $\bar{u}$ quark in the 3-, 4-, 5-, and 6-flavor schemes.

higher-order processes involving virtual quark loops; hence, it depends on the number of active quarks, and we make this dependence explicit with the $\alpha_S(\mu, N_F)$ notation. More precisely, the strong coupling depends on the renormalization scale μ_R, in contrast to the factorization scale μ_F. However, for this work we have set $\mu_R = \mu_F = \mu$.

In Fig. 4 we display $\alpha_S(\mu, N_F)$ vs μ for different N_F values. We choose an initial $\alpha_S(\mu, N_F)$ at a low $\mu = Q_0$ and $N_F = 3$, and evolve this to larger scales using the NLO beta function. (See Appendix A 1 for details.) As we saw in Fig. 2, the N_F transitions are evident.

There are strong constraints on $\alpha_S(\mu, N_F)$ at low scales ($\mu \sim m_\tau$) from hadronic τ decays, and at high scales ($\mu \sim M_Z$) from LEP2 measurements [41]; thus, it is not trivial to satisfy both limits for a fixed value of N_F.

C. Interplay between $\alpha_S(\mu, N_F)$ and $g(x, \mu, N_F)$

If we could do an all-orders calculation for any physical observable, this would be independent of N_F and μ; for finite-order calculations, any residual μ and N_F dependence is simply an artifact of our truncated perturbation theory. Thus, the separate contributions of the perturbative QCD result must conspire to compensate the μ and N_F dependence to the order of the calculation.

For example, when we activate the charm PDF, we find the gluon PDF is decreased. Within the limits of the perturbation theory, we would expect that the decreased contribution from the gluon initiated processes would be (at least partially) compensated by the new charm initiated processes. This compensation mechanism is clearly evident for the calculation of F_2^{charm}; additionally, we find that because the gluon initiated and charm initiated contribution generally have opposite renormalization scale dependence, the resulting VFNS prediction is more stable in μ as compared to the FFNS result [6].

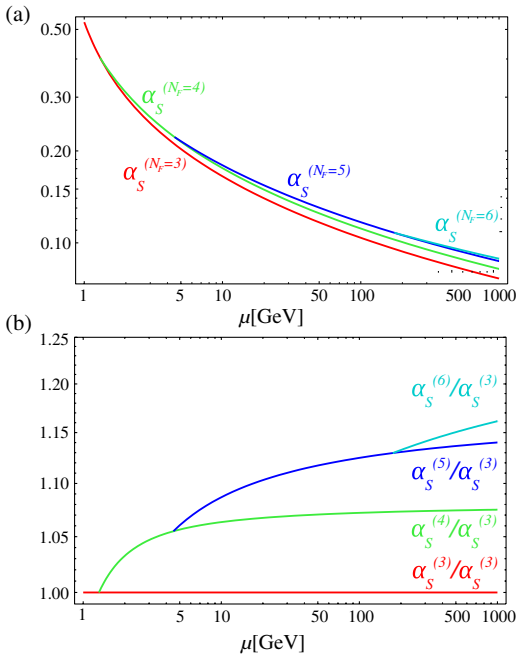

FIG. 4 (color online). (a) 2-loop α_S for different number of flavors; (b) ratio of 3-, 4-, 5-, and 6-flavor α_S to the 3-flavor one.

Another compensating mechanism is evident when comparing Figs. 2 and 4 where we note that the N_F dependence of α_s is generally opposite to that of the gluon PDF; this observation is particularly interesting as many NLO contributions are proportional to the combination $\alpha_S \times xg$. If we consider the inclusive structure functions F_{123L}, for example, the LO contributions are proportional to the electroweak couplings and the quark PDFs—both of which are relatively invariant under changes in N_F. Thus, the primary effect of the N_F dependence will be to modify the NLO contributions which are dominantly proportional to $\sim\alpha_S \times xg$. For these contributions, the xg and α_S dependence will partially cancel each other out so that the total result is relatively stable as a function of N_F [6,34].

To illustrate this mechanism, we show the combination $\alpha_S^{(N_R)} \times xg^{(N_F)}$ vs x (in Fig. 5) and vs μ (in Fig. 6).[14] The compensating properties are best observed in the ratio plots [Figs. 5(b) and 6(b)].

For example, in Fig. 5(b) for $\mu = 5$ GeV we see that if we start with $N_F = 3$ for both α_s and g (red line), the effect of changing $N_F = 5$ for α_s increases $\alpha_S \times xg$ by 6%; but, changing $N_F = 5$ for the gluon decreases $\alpha_S \times xg$ by roughly the same amount. Hence, the combination $\alpha_S \times xg$ is relatively stable under a change of N_F as we see by comparing the curves labeled $\{3, 3\}$ (red) and $\{5, 5\}$ (cyan). This is an example of how the perturbation theory adjusts to yield a result that is (approximately) independent of N_F at a given order of perturbation theory.

In Fig. 6 we show $\alpha_S \times xg$ vs μ for a choice of x values $\{10^{-1}, 10^{-3}, 10^{-5}\}$. While $\{3, 3\}$ (red) and $\{5, 5\}$ (cyan) results are roughly comparable for lower μ and higher x values (10^{-1}), for smaller x values and larger μ the shift in the gluon is not sufficient to compensate that of α_s.

Reviewing Fig. 5 in more detail, we observe that the N_F compensation works well for lower μ values $\sim(5, 10)$ GeV across a broad range of x. For $\mu =$ 5 GeV, the curves labeled $\{3, 3\}$ (red) and $\{5, 5\}$ (cyan) match within about $\sim$2% over much of the x

[14]Note that we use here a 3(5)-flavor α_S together with 5(3)-flavor PDFs only for illustrative purposes. In the actual implementation of the H-VFNS we always keep $N_R = N_F$.

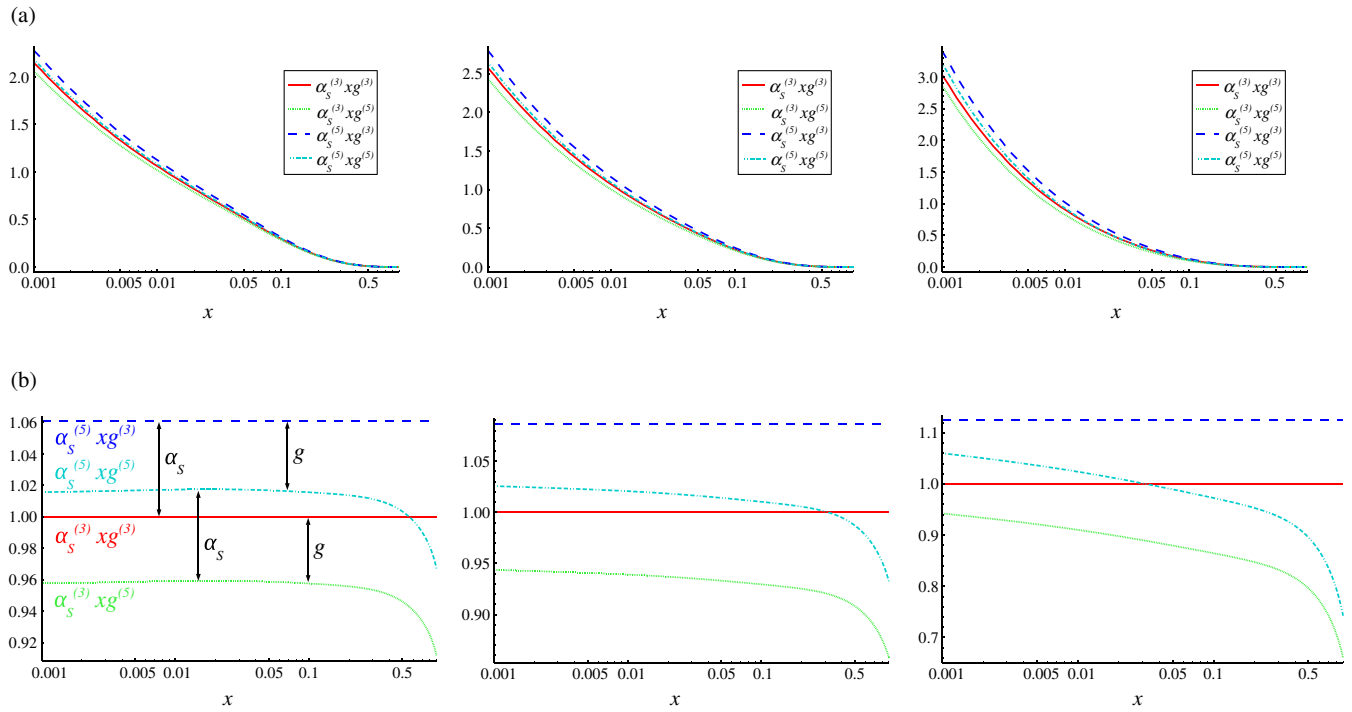

FIG. 5 (color online). $\alpha_S{}^{(N_R)}xg^{(N_F)}(x)$ as a function of x, for different values of μ. The curves are labeled $\alpha_S{}^{(N_R)}xg^{(N_F)}(x) = \{N_R, N_F\}$ where the first term in braces indicates the N_R for the α_s and the second indicates the N_F for g. (a) Different combinations of 3- and 5-flavor $\alpha_S{}^{(N_R)}xg^{(N_F)}(x)$ as a function of x, for different values of μ: 5 (left), 10 (middle) and 100 (right) GeV. (b) Ratio of different combination of 3- and 5-flavor $\alpha_S{}^{(N_R)}xg^{(N_F)}(x)$ and $\alpha_S{}^{(3)}xg^{(3)}(x)$ as a function of x, for different values of μ: 5 (left), 10 (middle) and 100 (right) GeV.

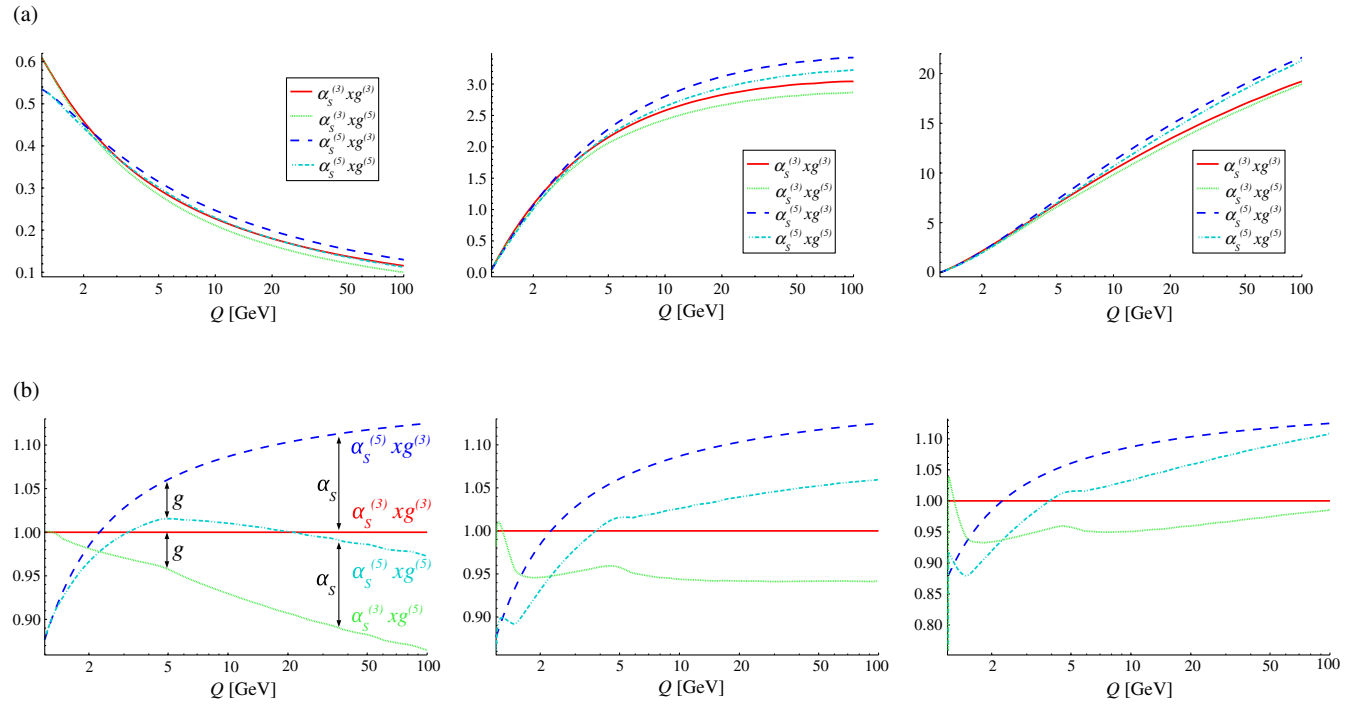

FIG. 6 (color online). $\alpha_S{}^{(N_R)}xg^{(N_F)}(x)$ as a function of μ, for different values of x. The curves are labeled $\alpha_S{}^{(N_R)}g^{(N_F)}(x) = \{N_R, N_F\}$ where the first term in braces indicates the N_R for the α_s and the second indicates the N_F for g. (a) Different combinations of 3- and 5-flavor $\alpha_S{}^{(N_R)}xg^{(N_F)}(x)$ as a function of μ, for different values of x : 10^{-1} (left), 10^{-3} (middle) and 10^{-5} (right). (b) Ratio of different combination of 3- and 5-flavor $\alpha_S{}^{(N_R)}xg^{(N_F)}(x)$ vs $\alpha_S{}^{(3)}xg^{(3)}(x)$ as a function of μ, for different values of x : 10^{-1} (left), 10^{-3} (middle) and 10^{-5} (right).

range. However, for larger $\mu = 100$ GeV the compensation between α_S and g is diminished. We will see this pattern again when we examine the physical structure functions, and this difference is driven (in part) by uncanceled mass singularities in the FFNS result.

V. PHYSICAL STRUCTURE FUNCTIONS VS N_F

Having examined the unphysical (but useful) combination $\alpha_S \times xg$, we now consider the physical observables F_2 and F_L vs N_F. In Fig. 7 we display F_2 vs Q for a choice of three x values; the absolute values are shown in the upper figures, and the ratios in the lower figures. Figure 8 shows

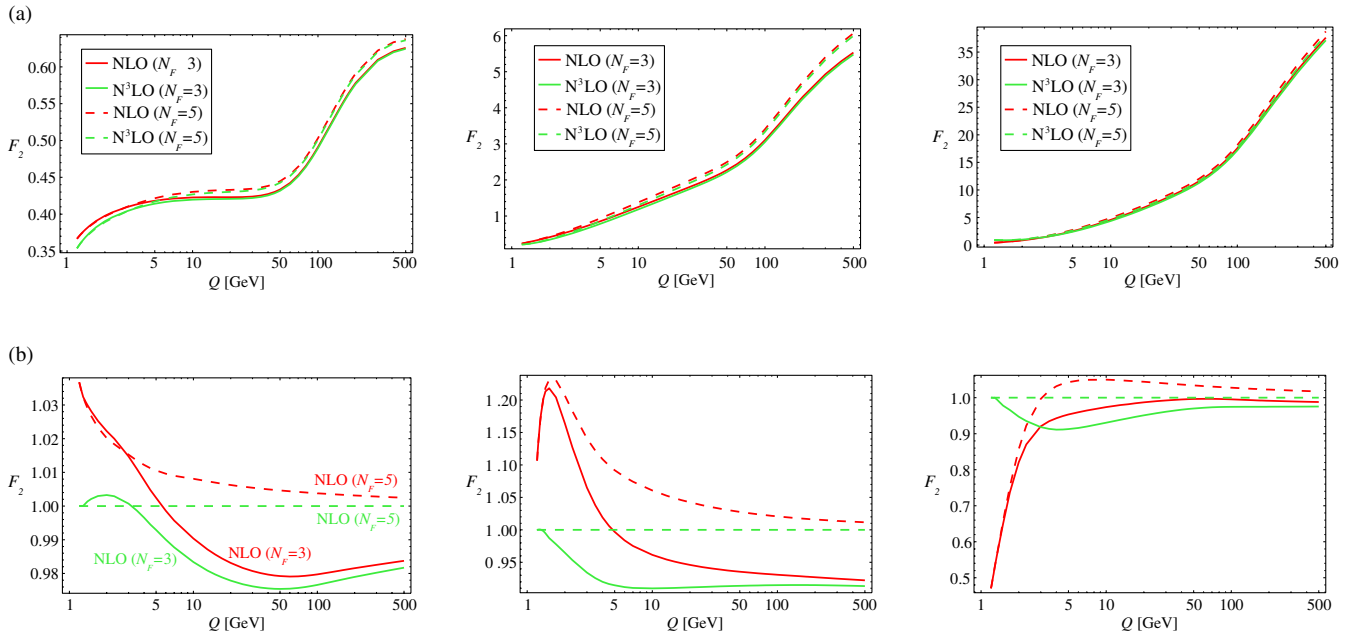

FIG. 7 (color online). (a) Inclusive F_2, (b) Ratio of inclusive F_2 as a function of Q [GeV] for different values of x : 10^{-1} (left), 10^{-3} (middle) and 10^{-5} (right). In these calculations we have chosen $\mu = Q$.

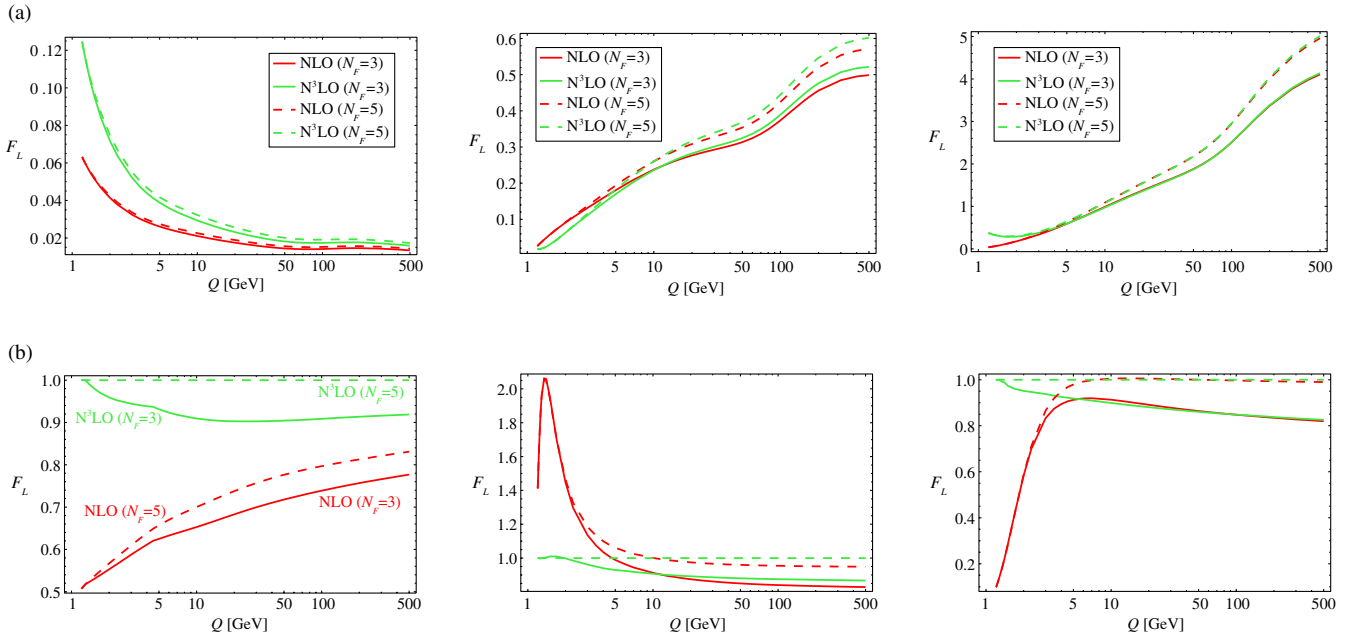

FIG. 8 (color online). (a) Inclusive F_L, (b) Ratio of inclusive F_L as a function of Q [GeV] for different values of x : 10^{-1} (left), 10^{-3} (middle) and 10^{-5} (right). In these calculations we have chosen $\mu = Q$.

the corresponding plots for F_L. Both F_2 and F_L were calculated at NLO and N3LO [11] using 3- and 5-flavor H-VFNS PDFs.[15] We observe a number of patterns in these figures.

A. Low Q: $Q < m$

At low Q values, the $N_F = 3$ and $N_F = 5$ results coincide. This is by design as once we go below the thresholds for $N_F = 4$, 5 the charm and bottom quarks are "deactivated" and all N_F calculations reduce to the $N_F = 3$ result.

At low Q values, we also observe there is a significant difference between the NLO and N3LO results; this difference arises from a number of sources including the fact that at low Q the value of α_s is large, hence the higher order corrections are typically larger here.

B. High Q: $Q \gg m$

As we move to larger Q values, we notice two distinct features.

First, at large Q we find the NLO and N3LO results tend to coincide.[16] Because α_s is decreasing at larger Q, the relative importance of the higher order corrections is reduced.

Second, we see that the $N_F = 3$ and $N_F = 5$ results slowly diverge from each other, both for the NLO and N3LO cases. This difference can be traced to the uncanceled mass singularity in the $N_F = 3$ calculations which is roughly proportional to $\alpha_s \ln[Q/m]$. In the $N_F = 5$ calculation, these logs are resummed into the heavy quark PDFs; for the $N_F = 3$ calculation, these logs are not resummed and the calculation will be divergent in the limit $Q/m \to \infty$.

C. Intermediate Q: $Q \gtrsim m$

We now come to the critical question: how far above the charm flavor transition can we extend the $N_F = 3$ FFNS calculation before the uncanceled logs $\alpha_s \ln[Q/m]$ degrade the perturbation expansion. By examining Figs. 7 and 8 we can determine the extent to which the $N_F = 3$ and $N_F = 5$ results diverge due to these logs. For scales $\mu = Q$ a few times the quark mass (m_c) the difference is small; but for larger scales $\mu = Q \sim 10 m_c$ the difference can be in excess of 10% depending on the specific x region. Also note that while we are considering the inclusive $F_{2,L}$, it is only the heavy quark components which are driving the difference at large μ scales; for a less inclusive observable (such as F_2^{charm}) this effect would be even more prominent.

1. Recap

To recap, in the three kinematic regions of interest we find the following.

$Q < m$ In the low Q region, we find the $N_F = 3$ and $N_F = 5$ results coincide; hence, in this region an $N_F = 3$ FFNS result will match with any VFNS result. Thus, we can use either the $N_F = 3$ and $N_F = 5$ calculation in this region.

$Q \gg m$ In the region of high Q, we find the $N_F = 3$ and $N_F = 5$ results diverge logarithmically due to the uncanceled mass singularities, and in the limit $Q/m \to \infty$ the $N_F = 3$ calculation contains divergent terms. Hence, in this region, we would expect the VFNS $N_F = 5$ result to be most reliable.

$Q \gtrsim m$ For Q scales which are a few times the quark mass or less, the $N_F = 3$ and $N_F = 5$ results are comparable; for larger Q scales, this difference will increase logarithmically with the scale. Thus, we can use either the $N_F = 3$ and $N_F = 5$ calculation in this region, but as we move to larger scales we need to transition to the $N_F = 5$ in the VFNS.

These conclusions are illustrated in Fig. 1, and now we are able to make quantitative statements about the specific regions of validity.

In summary, the N_F-dependent PDFs provide us the freedom to choose the N_F transitions where it is convenient for the analysis of specific data sets; however, this freedom comes with the responsibility that we must be aware of the mass singular logs and be sure not to extend a particular N_F FFNS calculation beyond its region of reliability.

VI. AN EXAMPLE: FROM LOW TO HIGH SCALES

We now finish with an example of how the H-VFNS scheme could be employed for a simultaneous study of both a low-scale process ($\mu \sim m_b$) at HERA[17] and a high-scale process ($\mu \gg m_{c,b}$) at the LHC.[18]

At HERA, a characteristic Q range for the extraction of F_2^{charm}, for example, is $\sim 2 < Q < 10$ GeV and this spans the kinematic region where the charm and bottom quarks become active in the PDF. These analyses can be performed using a $N_F = 3$ FFNS calculation as the scales involved are not particularly large compared to the $m_{c,b,}$ scales. Additionally, the extraction of the F_2^{charm} structure function is often computed using the HVQDIS program [51], and this explicitly works in a $N_F = 3$ FFNS. This

[15] As there is no complete N3LO massive calculation, we are using the approximation of Ref. [11]; this is entirely sufficient for the purposes of this study. Note that in Ref. [11], the PDF evolution is performed at NNLO by the QCDNUM [43] code which implements the $\overline{\text{MS}}$ matching conditions [44] which includes the resulting discontinuities.

[16] The one exception is F_L at large x values; this suggests that the higher order corrections in this kinematic region are large. Recall that in the limit $m/Q \to 0$ the LO contribution to F_L vanishes, so it is not entirely surprising that this has large higher order contributions.

[17] A relevant data set could be the recent analysis [48] by the H1 experiment of $D^{*\pm}$ meson production and the extracted F_2^{charm} structure function.

[18] A relevant data set could be, for example, high-mass dilepton resonances [49] or dijet mass spectrum [50]; both analyses extend beyond one TeV.

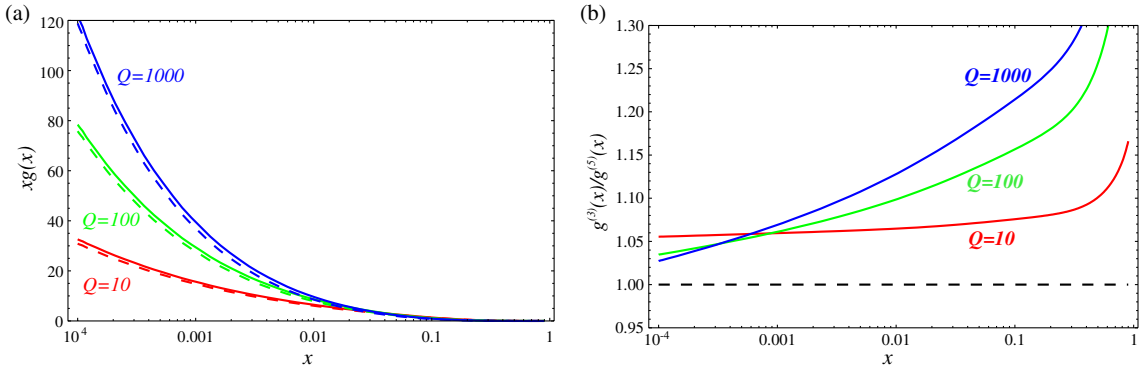

FIG. 9 (color online). (a) Comparison of 3-flavor (solid lines) and 5-flavor (dashed lines) gluon for $Q = \{10, 100, 1000\}$ GeV. (b) Ratio of 3- to 5-flavor gluon for the corresponding Q values.

approximation is entirely adequate in this kinematic region as resummed logs are not particularly large in the relevant Q region. The F_2^{charm} structure function extracted in [48] is compared with predictions using $N_F = 3$ FFNS PDFs from CT10f3 [1] and MSTW2008f3 [40] and both yield good descriptions of the data.

Conversely, at the LHC the μ range for new particle searches via the Drell-Yan process can be in excess of a TeV. For this analysis, we would want to use $N_F = 5$ so that the charm and bottom logs are resummed.[19]

Because the H-VFNS simultaneously provides $N_F = \{3, 4, 5, 6\}$, we can analyze the HERA data in a FFNS $N_F = 3$ context while also analyzing the LHC data in a $N_F = \{4, 5, 6\}$ VFNS context.

Operationally, we could perform a PDF fit to both a combination of HERA and LHC data by implementing the following steps.

(1) Parametrize the PDFs at a low initial scale $\mu = Q_0 \sim 1$ GeV, and generate a family of N_F-dependent PDFs as outlined in Sec. III A.
(2) Fit the HERA F_2^{charm} structure function data using $N_F = 3$ "FFNS" PDFs, $f_i(x, \mu, N_F = 3)$ and $\alpha_s(\mu, N_F = 3)$.
(3) Fit the high-scale LHC data using $N_F = 4, 5, 6$ "VFNS" PDFs, $f_i(x, \mu, N_F = 4, 5, 6)$ and $\alpha_s(\mu, N_F = 4, 5, 6)$.
(4) Repeat steps (1) through (3) until we have a suitable minimum.

Note, because we generate all the PDFs and α_s for all $N_F = \{3, 4, 5, 6\}$ flavors in step (1), the separate N_F branches are analytically related. Furthermore, this is done using a "forward" DGLAP evolution; no "backward" DGLAP evolution is required.

Also note that because we have access to all $N_F = \{3, 4, 5, 6\}$ sets, there is no difficulty in performing the HERA analysis of step (2) and the LHC analysis of step (3) in different N_F frameworks.

[19]We could also use $N_F = 6$, but the difference with the $N_F = 5$ case is minimal.

Finally, as we demonstrated in Sec. V, the user is now responsible for ensuring each N_F calculation is not used beyond its range of validity. While it is now possible to compute with $N_F = 3$ at high μ scales, this does not necessarily give a reliable result for the cross sections.

A. N_F conversion factors

Finally, we demonstrate how to use the family of N_F-dependent PDFs to estimate the effect of changing from $N_F = 3$ to $N_F = 5$ in a calculation such as the extraction of F_2^{charm} discussed above. For example, the HVQDIS program [51,52] works in an $N_F = 3$ FFNS while many of the PDFs are only available for $N_F = 4$, 5. If we have access to both $N_F = 3$ and $N_F = 5$ PDFs, we can simply use the correct N_F PDF set, and the conversion between the different N_F sets is simply given by the following identity:

$$f^{(N_F=5)}(x) = f^{(N_F=3)}(x)\left[\frac{f^{(N_F=5)}(x)}{f^{(N_F=3)}(x)}\right].$$

The term in brackets above represents the "correction factor" in converting between $N_F = 3$ and $N_F = 5$ PDF sets.

As we noted in Sec. IV A, the dominant effect of changing from $N_F = 3$ to $N_F = 5$ was to deplete the gluon PDF which fed the charm PDF via the $g \to c\bar{c}$ process. Therefore, we can estimate this effect by comparing the shift of the gluon PDF for $N_F = 3$ and $N_F = 5$. This effect is shown in Fig. 9(a) where we plot the gluon PDF explicitly, and in Fig. 9(b) we plot the ratio. We see that even at the lowest Q value displayed (10 GeV) the shift in the gluon PDF is $\sim$6% and relatively insensitive to x, except for the highest x values. Because the x dependence is minimal, we can approximately extract this correction factor from the convolution of the PDFs; thus, at scales $\mu \lesssim 10$ GeV, we can estimate the effect of the $N_F = 3$ to $N_F = 5$ conversion by simply rescaling the gluon PDF.

For example, if we are looking at charm structure functions, this is driven by the $\gamma g \to c\bar{c}$ process, plus

higher order corrections. Since this process is linear in the gluon PDF, the effect would be approximately a constant overall shift; specifically, 6% for the case of $Q \sim 10$ GeV.

Even if we do not have access to both the $N_F = 3$ and $N_F = 5$ PDF sets, the combination $[f^{(N_F=5)}/f^{(N_F=3)}]$ is driven by the DGLAP evolution and only mildly sensitive to the detailed PDF; hence, the above technique can still provide a rough approximation as to the correction factor between the $N_F = 3$ and $N_F = 5$ PDFs.

VII. CONCLUSION

We have investigated the N_F dependence of the PDFs and proposed an extension of the traditional VFNS which we denote the H-VFNS. In this scheme, we include an explicit N_F dependence in both the PDFs $f_a(x, \mu, N_F)$ and strong coupling $\alpha_S(\mu, N_F)$; this provides the user the freedom, and responsibility, to choose the appropriate N_F values for each data set and kinematic region.

Our H-VFNS implementation economically requires only four PDF grids (for $N_F = \{3, 4, 5, 6\}$), yet provides the user flexibility to use any switching scale. For a practical implementation of the H-VFNS, we choose a fixed matching scale $\mu_M^{(N_F)} = m_{N_F}$ and demonstrate that this has minimal impact on the physical results.

The H-VFNS is able to simultaneously work with low energy data (e.g., HERA data at low Q^2) in a $N_F = 3$ FFNS framework, while also incorporating high-scale LHC data in an $N_F = \{3, 4, 5, 6\}$ framework. Additionally, this can be implemented without any backward DGLAP evolution.

Although the PDFs and $\alpha_S(\mu, N_F)$ are discontinuous across flavor thresholds at higher orders, the H-VFNS provides the user the flexibility to shift the N_F transition for individual data sets and kinematic regions to avoid complications.

Thus, the H-VFNS provides a valuable tool for fitting data across a wide variety of processes and energy scales from low to high.

ACKNOWLEDGMENTS

We thank Sergey Alekhin, Michiel Botje, John Collins, Kateria Lipka, Pavel Nadolsky, Voica Radescu, Randall Scalise, and the members of the HERA-Fitter group for valuable discussions. F. I. O., I. S., and J. Y. Y. acknowledge the hospitality of CERN, DESY, Fermilab, and Les Houches where a portion of this work was performed. This work was partially supported by the U.S. Department of Energy under Grant No. DE-FG02-13ER41996, and the Lighter Sams Foundation. The research of T. S. is supported by a fellowship from the Théorie LHC France initiative funded by the CNRS/IN2P3. This work has been supported by *Projet international de cooperation scientifique* PICS05854 between France and the U.S. T. J. was supported by the Research Executive Agency (REA) of the European Union under the Grant Agreement No. PITN-GA-2010-264564 (LHCPhenoNet).

APPENDIX: EVOLUTION AND MATCHING CONDITIONS

1. α_S evolution and matching conditions

The running of the $\alpha_S(\mu, N_F)$ is given by the renormalization group equation:

$$\mu^2 \frac{d\alpha_s}{d\mu^2} = \beta(\alpha_s) = -(b_0\alpha_s^2 + b_1\alpha_s^3 + b_2\alpha_s^4 + \cdots).$$

At the NLO (2-loop) level, which we use in this work, we obtain

$$\alpha_S(\mu^2, N_F) = \frac{1}{b_0 \ln\frac{\mu^2}{\Lambda^2}}\left(1 - \frac{b_1}{b_0^2}\frac{\ln\left(\ln\frac{\mu^2}{\Lambda^2}\right)}{\ln\frac{\mu^2}{\Lambda^2}}\right), \quad \text{(A1)}$$

where $b_0 = (33 - 2N_F)/12\pi$ and $b_1 = (153 - 19N_F)/24\pi^2$. The N_F dependence arises from the virtual quark loops which enter at higher orders.

The relation of α_s across flavor thresholds for N_F and $N_F + 1$ flavors is computed to be [41]

$$\alpha_S(\mu^2, N_{F+1}) = \alpha_S(\mu^2, N_F)\left[1 + \sum_{k=1}^{\infty}\sum_{\ell=0}^{k} c_{k\ell}[\alpha_S(\mu^2, N_F)]^k \ln^l\left(\frac{\mu^2}{m^2}\right)\right],$$

where $c_{10} = 0$ and $c_{20} = -11/72\pi^2$. Thus, even if we perform the matching at $\mu = m$ we find

$$\alpha_S(m^2, N_F + 1) = \alpha_S(m^2, N_F) + c_{20}\alpha_S^3(m^2, N_F)$$

such that there is an $\mathcal{O}(\alpha_S^3)$ discontinuity in α_S.

In the above, the μ scale appearing in the argument of α_S is more precisely the renormalization scale μ_R; this is distinguished from the factorization scale μ_F appearing in the argument of PDF. However, in this work, we choose to set $\mu_R = \mu_F = \mu$.

Note also that there are in fact two versions of the FFNS scheme, which are characterized by different treatments of the number of active flavors entering α_S (denoted here as N_R, to be distinguished from the number of flavors entering PDF evolution N_F). In the "classical" FFNS, $N_R = N_F$. In the modified version, N_R is incremented across flavor thresholds as in the VFNS while N_F remains fixed. Discussion of advantages and disadvantages of these two formulations of FFNS can be found in [39,53]. In particular, allowing N_R to vary can help the running α_S accommodate experimental constraints from both high ($\sim M_Z$) and low ($\sim m_\tau$) scales [41,54].

2. PDF evolution and matching conditions

The relation of the PDFs with $N_F + 1$ flavors to that of N_F can be computed perturbatively [44,55]. The explicit form of these matching conditions can be found e.g. in

Eqs. (2.37)–(2.41) and Appendix B of Ref. [44]. For the purpose of further discussion we show here only a symbolic form of the matching conditions

$$\tilde{f}_i(x,\mu,N_F+1) = A^{ij}\otimes \tilde{f}_j(x,\mu,N_F), \tag{A2}$$

where

$$A^{ij} = \delta^{ij} + \frac{\alpha_S}{2\pi}\left(a_1^{ij} + b_1^{ij}\ln\left[\frac{\mu^2}{m^2}\right]\right) + \left(\frac{\alpha_S}{2\pi}\right)^2\left(a_2^{ij} + b_2^{ij}\ln\left[\frac{\mu^2}{m^2}\right] + c_2^{ij}\ln^2\left[\frac{\mu^2}{m^2}\right]\right) + \cdots. \tag{A3}$$

In the above equation $\tilde{f}_i$ can be a combination of light parton densities $(f_i + f_{\bar{i}})$, heavy parton densities $(f_H + f_{\bar{H}})$, the singlet combination of parton densities Σ, or the gluon. Note that there is an implicit summation over the above combinations. Coefficients $a^{ij}, b^{ij}, \ldots$ can be computed perturbatively. While we have not indicated it explicitly, all quantities on the right-hand side of Eq. (A2) [including $\alpha_S(N_F)$] are evaluated with N_F flavors, and those on the left-hand side are evaluated with N_F+1 flavors.

Note that the QCDNUM [43] program includes the NNLO evolution with the discontinuous and NNLO matching conditions.

In the $\overline{\text{MS}}$ scheme the a_1^{ij} term is computed to be zero, while the a_2^{ij} term is nonzero. Because $a_1^{ij}=0$, if we perform the matching between N_F and N_F+1 flavors at $\mu = m$, the $\ln(\mu/m)$ terms vanish and we find at NLO $[\mathcal{O}(\alpha_S{}^1)]$ that $f_i(x,\mu=m,N_F+1) = f_i(x,\mu=m,N_F)$; that is, the PDFs are continuous. This is why, at NLO, the VFNS implemented the matching automatically at $\mu = m$. Because $a_2^{ij}\neq 0$, at NNLO and beyond the PDFs will acquire discontinuities of $\mathcal{O}(\alpha_S{}^2)$; therefore, there is no longer any special benefit obtained by forcing the N_F transition at $\mu = m$.

For example, the discontinuity of the b-quark PDF is shown in Fig. 10(a), and curiously this yields a slightly negative value just above the transition point for $f_b(x,\mu \gtrsim m, N_F=5)$. There is a corresponding discontinuity in the gluon PDF (not shown) which has a positive shift, as it must to ensure the PDF sum rules are satisfied.

These discontinuities exhibit themselves in the physical observables such as the structure functions as shown in Figs. 10(b) and 10(c). These discontinuities are formally higher order, and will be reduced order by order as we extend the perturbation theory. It is interesting to note that F_L for the larger x value (10^{-3}) has a slightly positive discontinuity while at the smaller x value (10^{-5}) the discontinuity is negative. This reflects the shift between the (positive) gluon and the (negative) quark contributions in the different x regions. It is this mixture of the gluon and the quark terms which will ensure the physical observable is continuous up to the specified order of perturbation theory, while the PDF will always remain discontinuous at $\mathcal{O}(\alpha_S{}^2)$.

In the presented H-VFNS, we choose to compute the matching between N_F and N_F+1 flavors at $\mu = m$ (because the logs vanish); however, since we retain both the N_F and N_F+1 PDFs for $\mu \geq m$, the user has the choice to compute in either the N_F or N_F+1 framework, whichever is more suitable. Because the traditional VFNS did not provide PDFs for N_F flavors at $\mu \geq m$, this was previously not an option.

The matching conditions of Eqs. (A2) and (A3) essentially represent a perturbative expansion of the DGLAP evolution equations, up to an additional constant term a_k^{ij}.

We observe that if we choose to perform the matching not at $\mu = m$ but instead at a higher scale such as $\mu = 2m$, the PDF boundary condition for the heavy quark is not $f_c(x,\mu,N_F=4)=0$. Instead, the correct condition at NLO is

$$f_c(x,\mu,N_F=4) \simeq 0 + \frac{\alpha_S(\mu,N_F=3)}{2\pi} \times \ln\left[\frac{\mu^2}{m_c^2}\right] P_{qg}\otimes g(x,\mu,N_F=3) + \cdots. \tag{A4}$$

Note, the left-hand side uses $N_F=4$ PDFs and the right-hand side uses $N_F=3$ PDFs.

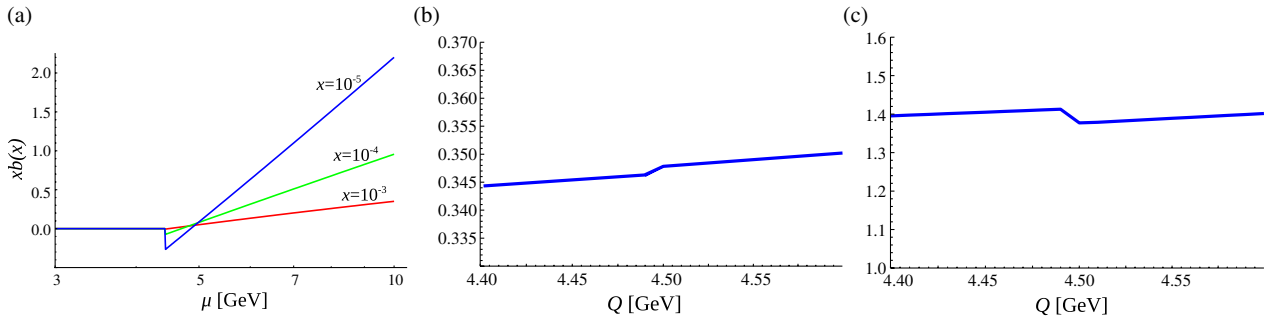

FIG. 10 (color online). (a) Discontinuity in the b-quark PDF $f_b(x,\mu)$ at NNLO vs μ for $x=\{10^{-3},10^{-4},10^{-5}\}$. (b), (c) Discontinuity for F_L vs Q for $x=\{10^{-3},10^{-5}\}$ (left to right) at NNLO in the region of the bottom mass, $m_b = 4.5$ GeV, as computed in Ref. [11].

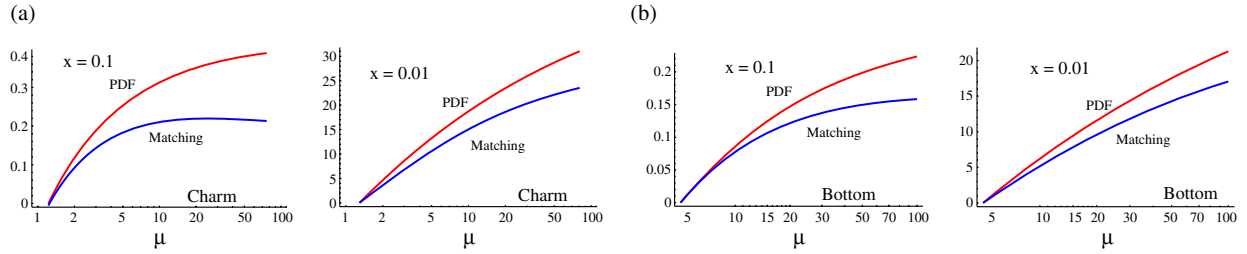

FIG. 11 (color online). Comparison of (a) charm and (b) bottom matching conditions at NLO with the DGLAP evolved PDFs for $x = \{0.1, 0.01\}$.

These matching conditions are displayed in Fig. 11 where we compare these to the DGLAP evolved PDF distribution at NLO. We see for scales near the matching point $\mu \sim m$, the differences are small. However, if the matching is performed away from the $\mu \sim m$ region, then the differences are larger. This is because the matching of Eq. (A4) is only computed to NLO, so it only includes a single partonic splitting, while the DGLAP evolution resums an infinite tower of partonic emissions. The difference comes from the missing second-order splittings which are proportional to ${\alpha_S}^2 \ln(\mu/m)$. If we repeat this exercise and compute the matching to NNLO,[20] then we will include the ${\alpha_S}^2 \ln(\mu/m)$ contributions, but miss the ${\alpha_S}^3 \ln(\mu/m)$. Thus the curves in Fig. 11 will remain comparable for a larger range of $\mu \gtrsim m$.

[20]An example of NNLO matching is provided in Ref. [22].

In this analysis, our matching scale is always taken to be the quark mass, $\mu_M^{(N_F)} = m_{N_F}$. This provides us the benefit that the PDF with N_F active flavors is defined for all values above $\mu = m_{N_F}$ without invoking backward evolution.

In the traditional VFNS, the switching scale $\mu_S^{(N_F)}$ was forced to be equal to the matching scale, which was set to the quark masses: $\mu_S^{(N_F)} = \mu_M^{(N_F)} = m_{N_F}$. For the H-VFNS, the switching scale $\mu_S^{(N_F)}$ is not predefined by the PDF set but can freely be chosen by the user.

The resulting PDFs will, to some extent, depend on the matching scale $\mu_M^{(N_F)}$, but as Fig. 11 demonstrates this effect will be insignificant so long as $\mu_M^{(N_F)} \sim m_{N_F}$. Likewise, resulting observables will, to some extent, depend on the switching scale $\mu_S^{(N_F)}$, but as Figs. 7 and 8 demonstrate, this effect will be insignificant so long as we do stay within the region of validity.

[1] H.-L. Lai, M. Guzzi, J. Huston, Z. Li, P. M. Nadolsky, J. Pumplin, and C.-P. Yuan, Phys. Rev. D **82**, 074024 (2010).
[2] J. Gao *et al.*, arXiv:1302.6246.
[3] I. Schienbein, J. Yu, C. Keppel, J. Morfín, F. Olness, and J. Owens, Phys. Rev. D **77**, 054013 (2008).
[4] I. Schienbein, J. Yu, K. Kovařík, C. Keppel, J. Morfín, F. Olness, and J. Owens, Phys. Rev. D **80**, 094004 (2009).
[5] M. A. G. Aivazis, F. I. Olness, and W.-K. Tung, Phys. Rev. D **50**, 3085 (1994).
[6] M. Aivazis, J. C. Collins, F. I. Olness, and W.-K. Tung, Phys. Rev. D **50**, 3102 (1994).
[7] M. Kramer, F. I. Olness, and D. E. Soper, Phys. Rev. D **62**, 096007 (2000).
[8] W.-K. Tung, S. Kretzer, and C. Schmidt, J. Phys. G **28**, 983 (2002).
[9] S. Kretzer and I. Schienbein, Phys. Rev. D **58**, 094035 (1998).
[10] M. Guzzi, P. M. Nadolsky, H.-L. Lai, and C.-P. Yuan, Phys. Rev. D **86**, 053005 (2012).
[11] T. Stavreva, F. I. Olness, I. Schienbein, T. Ježo, A. Kusina, K. Kovařík, and J. Y. Yu, Phys. Rev. D **85**, 114014 (2012).
[12] P. Kotko and W. Slominski, Phys. Rev. D **86**, 094008 (2012).
[13] P. Kotko and W. Slominski, arXiv:1206.3517.
[14] B. Kniehl, G. Kramer, I. Schienbein, and H. Spiesberger, Phys. Rev. D **84**, 094026 (2011).
[15] A. D. Martin, W. J. Stirling, R. S. Thorne, and G. Watt, Eur. Phys. J. C **63**, 189 (2009).
[16] R. S. Thorne and R. G. Roberts, Phys. Rev. D **57**, 6871 (1998).
[17] R. Thorne, Phys. Rev. D **73**, 054019 (2006).
[18] M. Cacciari, M. Greco, and P. Nason, J. High Energy Phys. 05 (1998) 007.
[19] S. Forte, E. Laenen, P. Nason, and J. Rojo, Nucl. Phys. **B834**, 116 (2010).
[20] R. D. Ball, V. Bertone, F. Cerutti, L. Del Debbio, S. Forte, A. Guffanti, J. I. Latorre, J. Rojo, and M. Ubiali, Nucl. Phys. **B849**, 296 (2011).
[21] R. D. Ball *et al.*, Nucl. Phys. **B867**, 244 (2013).

[22] S. Alekhin, J. Blumlein, S. Klein, and S. Moch, Phys. Rev. D **81**, 014032 (2010).

[23] S. Alekhin, J. Blumlein, and S. Moch, Phys. Rev. D **86**, 054009 (2012).

[24] M. Gluck, P. Jimenez-Delgado, and E. Reya, Eur. Phys. J. C **53**, 355 (2008).

[25] P. Jimenez-Delgado and E. Reya, Phys. Rev. D **79**, 074023 (2009).

[26] R. Thorne and W. Tung, arXiv:0809.0714.

[27] F. Olness and I. Schienbein, Nucl. Phys. Proc. Suppl. B **191**, 44 (2009).

[28] J. Andersen *et al.* (SM and NLO Multileg Working Group), arXiv:1003.1241.

[29] J. C. Collins, Phys. Rev. D **58**, 094002 (1998).

[30] J. Amundson, F. I. Olness, C. Schmidt, W. Tung, and X. Wang, *Theoretical Description of Heavy Quark Production in DIS* (1998), http://lss.fnal.gov/archive/1998/conf/Conf-98-153-T.pdf.

[31] J. C. Collins and W.-K. Tung, Nucl. Phys. **B278**, 934 (1986).

[32] F. I. Olness and R. J. Scalise, Phys. Rev. D **57**, 241 (1998).

[33] P. M. Nadolsky and W.-K. Tung, Phys. Rev. D **79**, 113014 (2009).

[34] F. I. Olness, R. Scalise, and W.-K. Tung, Phys. Rev. D **59**, 014506 (1998).

[35] B. Kniehl, G. Kramer, I. Schienbein, and H. Spiesberger, Phys. Rev. D **71**, 014018 (2005).

[36] B. Kniehl, G. Kramer, I. Schienbein, and H. Spiesberger, Eur. Phys. J. C **41**, 199 (2005).

[37] B. A. Kniehl, G. Kramer, I. Schienbein, and H. Spiesberger, Phys. Rev. D **77**, 014011 (2008).

[38] H. Lai, J. Huston, S. Kuhlmann, J. Morfin, F. Olness, J. F. Owens, J. Pumplin, and W. K. Tung (CTEQ Collaboration), Eur. Phys. J. C **12**, 375 (2000).

[39] A. Martin, W. Stirling, and R. Thorne, Phys. Lett. B **636**, 259 (2006).

[40] A. Martin, W. Stirling, R. Thorne, and G. Watt, Eur. Phys. J. C **70**, 51 (2010).

[41] J. Beringer *et al.* (Particle Data Group), Phys. Rev. D **86**, 010001 (2012).

[42] A. Aktas *et al.* (H1 Collaboration), Eur. Phys. J. C **45**, 23 (2006).

[43] M. Botje, Comput. Phys. Commun. **182**, 490 (2011).

[44] M. Buza, Y. Matiounine, J. Smith, and W. L. van Neerven, Eur. Phys. J. C **1**, 301 (1998).

[45] R. Thorne, Phys. Rev. D **86**, 074017 (2012).

[46] R. D. Ball *et al.* (NNPDF Collaboration), Phys. Lett. B **723**, 330 (2013).

[47] K. Kovarik, I. Schienbein, F. I. Olness, J. Y. Yu, C. Keppel, J. G. Morfín, J. F. Owens, and T. Stavreva, Phys. Rev. Lett. **106**, 122301 (2011).

[48] F. Aaron *et al.* (H1 Collaboration), Eur. Phys. J. C **71**, 1769 (2011).

[49] ATLAS Collaboration, Report No. ATLAS-CONF-2013-017, 2013.

[50] S. Chatrchyan *et al.* (CMS Collaboration) Phys. Rev. D **87**, 114015 (2013).

[51] B. Harris and J. Smith, Phys. Rev. D **57**, 2806 (1998).

[52] B. Harris and J. Smith, Nucl. Phys. **B452**, 109 (1995).

[53] M. Gluck and E. Reya, Mod. Phys. Lett. A **22**, 351 (2007).

[54] E. L. Berger, M. Guzzi, H.-L. Lai, P. M. Nadolsky, and F. I. Olness, Phys. Rev. D **82**, 114023 (2010).

[55] M. Buza, Y. Matiounine, J. Smith, R. Migneron, and W. van Neerven, Nucl. Phys. **B472**, 611 (1996).